AIAA JOURNAL
Vol. 33, No. 8, August 1995

Transition Model for High-Speed Flow

Eric S. Warren*
North Carolina State University, Raleigh, North Carolina 27695-7910
Julius E. Harris†
NASA Langley Research Center, Hampton, Virginia 23681
and
H. A. Hassan‡
North Carolina State University, Raleigh, North Carolina 27695-7910

A transition model for low-speed flows has previously been developed by Young et al. which incorporates first-mode (Tollmien–Schlichting) disturbance information from linear stability theory. The present work extends the model to high-speed flows by incorporating the effects of second-mode disturbances. The transition model is incorporated into a Reynolds-averaged Navier–Stokes solver with a one-equation turbulence model. Results using a variable turbulent Prandtl number approach demonstrate that the current model accurately reproduces available experimental data for first- and second-mode dominated transitional flows. The performance of the present model shows significant improvement over previous transition modeling attempts.

Introduction

THE study of high-speed transition is very important for the efficient design of hypersonic vehicles. Hypersonic vehicles, such as the National Aerospace Plane (NASP), encounter flows which may be transitional over a significant portion of the vehicle. Within this transitional region, design parameters such as skin friction, heat transfer, etc. are rapidly increasing or are maximum. Because of the current limitations of supercomputers, the most practical method for describing such flows are methods based on the Reynolds-averaged Navier–Stokes (RANS) equations. Traditionally, transition models based on the Reynolds-averaged equations have consisted primarily of the modification of existing turbulence models. The main objective of this work is the development of a transition model which incorporates information from linear stability theory and accurately reproduces available experimental data for transitional flows over a wide range of Mach numbers.

At Mach numbers less than about four, the transition process is dominated by first-mode disturbances. First-mode disturbances are vorticity disturbances which are characterized by fluctuations in velocity. First-mode disturbances in incompressible flows are known as Tollmien–Schlichting waves. At Mach numbers greater than four, the transition process is dominated by second-mode disturbances. Second-mode disturbances are acoustical disturbances which are characterized by large fluctuations in pressure and temperature, fluctuations which are much larger than the velocity fluctuations.

Previous work by Young et al.[1] has established a model for including the effects of first-mode disturbances into a transition model. The work by Young et al.[1] dealt exclusively with incompressible flows. An objective of the present work is the extension of this model to account for Mach number effects. Additionally, the present work includes the effects of second-mode disturbances which dominate the transition process at hypersonic speeds.

Received Nov. 22, 1993; revision received Nov. 14, 1994; accepted for publication Nov. 15, 1994.

*Research Assistant, Dept. of Mechanical and Aerospace Engineering. Student Member AIAA.

†Senior Research Scientist, Flow Modeling and Control Branch. Associate Fellow AIAA.

‡Professor, Dept. of Mechanical and Aerospace Engineering. Associate Fellow AIAA.

Formulation of the Problem

Transition Model

If Γ represents the fraction of the time the flow is turbulent, then the mean velocity, U_m is

$$U_m = \Gamma U_t + (1 - \Gamma)U_\ell \tag{1}$$

In Eq. (1) U_t is the mean turbulent velocity and U_ℓ is the mean nonturbulent or laminar velocity. Measurements by Kuan and Wang as cited in Ref. 1 showed that nonturbulent profiles are not Blasius profiles for flows over flat plates. Moreover, turbulent profiles are not the traditional fully developed profiles. At any given instant, the streamwise fluctuation in the transitional region u_r' is given by

$$u_r' = u - U_m$$

As shown in Ref. 1, the transitional stress can be written as

$$\overline{(u_i'u_j')_r} = \Gamma\overline{(u_i'u_j')_t} + (1 - \Gamma)\overline{(u_i'u_j')_\ell} + \Gamma(1 - \Gamma)\Delta U_i \Delta U_j \tag{2}$$

where

$$\Delta U_i = U_{t,i} - U_{\ell,i} \tag{3}$$

The expression shown in Eq. (2) is a result of three contributions: turbulent, nonturbulent, and a large-eddy component. Traditionally, transition models have only included the turbulent contribution, terms resulting from nonturbulent fluctuations have not been included. The terms $\Delta U_i \Delta U_j$ are a result of large eddies. Their calculation requires specification of the turbulent and nonturbulent profiles in the transitional region. For this work, the large-eddy term has been neglected.

The intermittency factor Γ is obtained from the expression developed by Dhawan and Narasimha,[2] i.e.,

$$\Gamma(x) = 1 - \exp(-0.412\xi^2) \tag{4}$$

with

$$\xi = (x - x_t)/\lambda$$

and λ is determined from the correlation

$$Re_\lambda = 9(Re_{x_t})^{0.75} \tag{5}$$

and x_t is value of x at the beginning of transition. Because of this, this model requires the specification of a transition "point." The

transition point can be determined from experiment or an e^n method.[3]

Turbulent Contribution

For a fully turbulent flow, all that is needed to close the RANS equation set is the turbulent Reynolds stress $\overline{\rho u_i'' u_j''}$ and the Reynolds heat flux $\overline{\rho u_j'' h''}$. By evaluating the turbulent Reynolds stress, the turbulent contribution to the general transitional stress is obtained. The turbulent contribution is the first term in Eq. (2)

The turbulent Reynolds stress is given in this work by Boussinesq's approximation which gives

$$-\overline{\rho u_i'' u_j''} = \mu_t \left(\frac{\partial \tilde{u}_i}{\partial x_j} + \frac{\partial \tilde{u}_j}{\partial x_i} - \frac{2}{3}\delta_{ij} \frac{\partial \tilde{u}_m}{\partial x_m} \right) - \frac{2}{3}\delta_{ij} \bar{\rho} \tilde{k} \tag{6}$$

where μ_t is the eddy viscosity and $\tilde{k}$ the turbulent kinetic energy per unit mass.

In this work, a one-equation model is used which specifies the eddy viscosity as

$$\mu_t = C_\mu \bar{\rho} \sqrt{\tilde{k}}\, \ell_\mu \tag{7}$$

where $C_\mu = 0.09$ is a model constant and ℓ_μ an algebraically derived length scale. This length scale is derived by considering the near-wall behavior of $\tilde{k}$ and characteristics of the log-law region in the turbulent velocity boundary layer. The turbulent viscous length scale ℓ_μ is given as

$$\ell_\mu = C_1 y \left[1 - \exp\left(-\frac{\sqrt{\tilde{k}}\, y}{C_2 \nu} \right) \right] \tag{8}$$

where

$$C_1 = (0.3)^{-\frac{3}{2}} \kappa \qquad C_2 = 70.0 \sqrt{T_w / T_{aw}} \tag{9}$$

and κ is the von Kármán constant (0.41). The length scale ℓ_μ contains a damping factor which takes into account the presence of the laminar sublayer in the turbulent velocity profile. The form of the length scale was originally derived by Mitcheltree et al.[4] for adiabatic walls. The correction $\sqrt{T_w/T_{aw}}$ is incorporated to allow for the presence of cooled walls.

Reynolds Heat Flux

In the energy equation, the quantity $\overline{\rho u_j'' h''}$ appears. This term is known as the Reynolds heat flux. This term is modeled by a gradient diffusion approximation, which gives

$$\overline{\rho u_j'' h''} = -C_p \alpha_t \bar{\rho} \frac{\partial \tilde{T}}{\partial x_j} \tag{10}$$

where α_t the turbulent diffusivity and C_p the specific heat at constant pressure. The turbulent diffusivity can be expressed in terms of the eddy viscosity and a turbulent Prandtl number Pr_t

$$\alpha_t = \nu_t / Pr_t \tag{11}$$

The resulting expression for the Reynolds heat flux becomes

$$\overline{\rho u_j'' h''} = -\frac{C_p \mu_t}{Pr_t} \frac{\partial \tilde{T}}{\partial x_j} \tag{12}$$

where μ_t is the eddy viscosity.

Traditionally, the turbulent Prandtl number is taken as a constant. The value of Pr_t varies in the literature but generally is chosen between 0.8 and 1.0. In this work, when the turbulent Prandtl number is chosen as a constant, the value is taken as 0.89. This was chosen to correspond to the value used in Ref. 5.

There are physical consequences in choosing Pr_t as a constant. By examining Eq. (12), it is clear that when Pr_t is a constant, the damping factor used is the same factor which appears in ℓ_μ. This is equivalent to treating the turbulent thermal boundary layer with the same damping as the turbulent velocity boundary layer, even though they have different laminar sublayer characteristics. As results will illustrate, this choice is inappropriate when considering quantities which are strong functions of the Prandtl number, such as the recovery factor.

Eddy-Diffusivity Model

It is possible to model the Reynolds heat flux in such a way that the turbulent temperature boundary layer is damped differently than the turbulent velocity boundary layer. Based on the variable turbulent Prandtl number approach of Cebeci,[6] the eddy-diffusivity model is assumed to have the form

$$\alpha_t = C_\mu \sqrt{\tilde{k}}\, \ell_T \tag{13}$$

The temperature length scale ℓ_T is assumed similar in form to the viscous and dissipation length scales and is given as

$$\ell_T = C_3 y \left[1 - \exp\left(-\frac{\sqrt{\tilde{k}}\, y}{C_4 \nu} \right) \right] \tag{14}$$

where

$$C_3 = 3.12 \qquad C_4 = 92.0$$

The constants C_3 and C_4 were determined by comparing with the experimental turbulent Prandtl number measurements of Meier and Rotta.[7]

By defining a separate length scale for the temperature boundary layer, different damping is obtained. The present eddy-diffusivity model implies a variable turbulent Prandtl number of the form

$$Pr_t = \ell_\mu / \ell_T \tag{15}$$

where ℓ_μ is the viscous length scale.

Nonturbulent Fluctuations

The second term in the general transitional stress

$$(1 - \Gamma)\overline{(u_i' u_j')_\ell} \tag{16}$$

is a result of laminar or nonturbulent fluctuations. As stated previously, this nonturbulent contribution has traditionally not been considered in RANS-type approaches. In this work, the nonturbulent fluctuations considered are a result of first- and second-mode disturbances.

First-Mode Disturbances

For moderate supersonic Mach numbers below approximately four, the dominant mode of instability is the first mode. The dominant disturbance frequency at breakdown is well predicted by the frequency of the first-mode disturbance having the maximum amplification rate. Using the work of Obremski et al.,[8] Walker[9] states that this frequency can be correlated by

$$\omega \nu / U_e^2 = 3.2 (Re_{\delta^*})^{-\frac{3}{2}} \tag{17}$$

where U_e is the velocity at the edge of the boundary layer, Re_{δ^*} the Reynolds number based on displacement thickness δ^*, and ω the frequency.

The preceding expression is valid for low-speed flow but can be extended, through the use of the reference temperature method, to high-speed flow. It is known[10] that compressible formulas for skin friction and heat transfer have the same form as the incompressible formulas provided the physical properties of the fluid are evaluated at some reference temperature between T_w and T_e. A possible definition of T^* is[11]

$$T^*/T_e = 1 + 0.032 M_e^2 + 0.58[(T_w/T_e) - 1] \tag{18}$$

where the e subscript denotes boundary-layer edge quantities and w denotes wall values. By using this reference temperature, Walker's

formula, i.e., Eq. (17), can be extended to higher Mach number flows by considering the definition of the unit Reynolds number as

$$Re^* = \rho^* U_\infty / \mu^* \tag{19}$$

with

$$\mu^* = \mu(T^*) \tag{20}$$

where T^* is the reference temperature evaluated from Eq. (18). The density can be approximated by noting

$$P_e/P^* = \rho_e R T_e / \rho^* R T^*$$

and assuming that the pressure is approximately constant throughout the boundary layer. As a result

$$\rho^*/\rho_e = T_e/T^* \tag{21}$$

The dominant first-mode frequency correlation can then be rewritten as

$$\omega \nu^* / U_e^2 = 3.2 (Re^*_{\delta^*})^{-\frac{3}{2}} \tag{22}$$

with δ^* also evaluated using Re^*.

By assuming a velocity scale of $\sqrt{\tilde{k}}$, the first-mode disturbance frequency ω can be used to define a length scale,

$$\ell_{\mathrm{TS}} = a\sqrt{\tilde{k}}/\omega \qquad a = 0.04 - 0.06 \tag{23}$$

For the model constant a, the value used in this work is 0.04. The value of 0.06 was used in Ref. 1 where the most amplified waves had a wave angle of zero. For compressible flows, the most amplified first-mode waves are oblique, with the wave angle ψ depending on the Mach number.[12] The value of 0.04 represents 0.06 cos ψ, where $\psi \approx 50$ deg. For transitional flows where the effects of the first mode are dominant, the turbulent and nonturbulent contributions to the stress tensor can be obtained by combining the two length scales as

$$\ell_\mu = (1 - \Gamma)\ell_{\mathrm{TS}} + \Gamma \ell^t_\mu \tag{24}$$

where ℓ^t_μ is the turbulent viscosity length scale. Thus, when $\Gamma = 0$, i.e., before transition,

$$\ell_\mu = \ell_{\mathrm{TS}}$$

Second-Mode Disturbances

Through the pioneering work of Mack,[12,13] the concept of second-mode disturbances was developed. As the boundary-layer edge velocity increases above approximately $M = 2.2$, a region of the boundary layer becomes supersonic relative to the phase velocity. Mack showed that when such a situation exists, multiple solutions to the inviscid stability equations arise. These additional solutions are called the higher modes. The first of these modes is called the second mode and is the most unstable of the higher modes, sometimes referred to as the Mack modes.

As the Mach number increases above four, the second-mode disturbances, which are higher frequency acoustical disturbances, dominate the transition process. From Mack[14] and Stetson and Kimmel,[15] the wave lengths of the most unstable second-mode disturbances have been shown to be about two boundary-layer thicknesses.

The frequency of the second mode disturbances can be written as

$$\omega_{\mathrm{SM}} = U_p/\lambda \tag{25}$$

where U_p is the phase velocity and λ the wavelength. For hypersonic boundary layers, this leads to the relationship

$$\lambda \propto 2\delta = \frac{c M_e^2 x}{\sqrt{Re_x}} \tag{26}$$

where c is a constant of proportionality. Combining with Eq. (25), the frequency is given as

$$\omega = \frac{U_p \sqrt{Re_x}}{c M_e^2 x} \tag{27}$$

Again defining a velocity scale as in Eq. (23), a second-mode contribution to the length scale can be defined as

$$\ell_{\mathrm{SM}} = b\frac{\sqrt{\tilde{k}}}{\omega}$$

which on substitution of Eq. (27) yields

$$\ell_{\mathrm{SM}} = \left(\frac{b}{U_p}\right) M_e^2 \sqrt{\frac{\tilde{k}x}{Re}} \tag{28}$$

By comparing with the Mach 8 stability experiment of Kimmel[16] and Ref. 17, the constant b was chosen as 0.23. Additionally, linear stability predicts the phase velocity to be about $0.94U_e$. Again, it is assumed that the second-mode contribution can be obtained by combining ℓ_{SM} into the viscous length scale giving

$$\ell_\mu = (1 - \Gamma)[\ell_{\mathrm{TS}} + \ell_{\mathrm{SM}}] + \Gamma \ell^t_\mu \tag{29}$$

Results and Discussion

Numerical Method

The numerical method used to solve the governing conservation equations and turbulent kinetic energy equation follows the method of Ref. 18 closely. A finite volume method was used to evaluate the spatial terms in the Navier–Stokes equations. The inviscid fluxes were computed by an upwind approach based on Roe's flux difference splitting. MUSCL differencing was used along with a min-mod flux limiter. Second-order central differencing was used to evaluate the viscous fluxes. The solution was stepped in time using a modified four-stage Runge–Kutta scheme until a steady state was obtained. The determination of a steady state was based on a density residual drop of five or more orders of magnitude. Because of the existence of a shock, grids of approximately 275 × 75 were needed to adequately resolve the shock and the very thin boundary-layer region. The steady state was obtained with run-times on the average of 3–4 Cray Y-MP h.

Because of the very large Reynolds numbers, as high as 8×10^7, the thin-layer Navier–Stokes equations were solved. The thin-layer approximation neglects streamwise derivatives in the viscous terms due to their small magnitude relative to the normal derivatives. This is a valid approximation since at very large Reynolds numbers the viscous effects are restricted to a very small region near a solid boundary. Because of the cell aspect ratios necessary to resolve this small region, streamwise derivatives in the viscous terms have a negligible contribution.

Experimental Data

To determine the accuracy of models, it is necessary to reproduce available experimental results. In the study of natural transition, flight data or data from quiet wind tunnels is necessary. The NASA Langley Mach 3.5 Pilot Low-Disturbance tunnel has emerged as the facility capable of reproducing transitional data of the quality that matches flight data. Using this tunnel, Chen et al.[3] presented recovery factor measurements on a 5-deg half-angle sharp cone and a flat plate. Three cases from these experiments are used for comparison with the present model. These are as follows.

Flow 3, case 5:

$$Re = 7.8 \times 10^7/\mathrm{m} \qquad x_t = 0.0815\ \mathrm{m}$$

Flow 3, case 6:

$$Re = 5.89 \times 10^7/\mathrm{m} \qquad x_t = 0.1174\ \mathrm{m}$$

Flow 3, case 7:

$$Re = 3.85 \times 10^7/\mathrm{m} \qquad x_t = 0.2166\ \mathrm{m}$$

with $L_{\mathrm{ref}} = 1$ m, $T_{\mathrm{ref}} = 98$ K, $M_{\mathrm{ref}} = 3.36$, and $q = 0.1\%$. The case designations are chosen to correspond to the same cases presented in Ref. 5. The reference quantities given are boundary-layer edge quantities. All of the data just given pertain to the cone experiments.

To determine the effect of the second-mode disturbances model, experiments at Mach numbers greater than four are necessary. Kimmel et al.[16] have carried out Mach 8 transition experiments over a flared and nonflared 7-deg half-angle cone. These experiments were carried out in the Arnold Engineering and Development Center (AEDC) tunnel B. The AEDC wind-tunnel is not a quiet tunnel in terms of freestream intensity levels. The freestream turbulence intensity level in the experiments[16] was around 3.0%, however, only a small portion of this was in the second-mode frequency range (frequencies above 80–100 kHz). Based on this, Ref. 15 states, "a conventional hypersonic wind tunnel can be quiet for second mode disturbances and noisy for first mode disturbances." The validity of this statement is still an open question. Regardless, at the present time, no second-mode dominated transition data obtained in quiet tunnels is available. Therefore, the present model is compared to these cases, which are given as follows.

Mach 8, flared:

$$M = 7.98 \qquad Re = 6562000/\text{m}$$

Mach 8, nonflared:

$$M = 7.98 \qquad Re = 6562000/\text{m}$$

Mach 9 data was added from a noisy tunnel at the suggestion of one of the reviewers. The tunnel in question is the Imperial College No. 2 Gun Tunnel.

Mach 3.5 Cases

The Mach 3.5 cases were used to determine the effectiveness of the transition model at predicting transitional flows which are characterized by first-mode dominated transition processes. Previous work by Young et al.[1] has established the capability of the model for low-speed flat plate flows. The Mach 3.5 cases studied were the ones carried out on the 5-deg half-angle cone. A flat plate case was also studied but was not presented here. The cone experiments measured the recovery factor by determining the surface temperature under adiabatic conditions.

The first set of results were obtained with the present model using a constant turbulent Prandtl number. The experimental data is from the flow 3, case 5 experiment which is the first experiment of the Chen et al.[3] set. Figure 1 compares the present model with the linear combination models as cited in Ref. 17. The computations with the linear combination models were carried out in Ref. 5 with a boundary-layer code. Linear combination models assume that the viscosity can be expressed as

$$\mu = \mu_l + \Gamma \mu_t \tag{30}$$

The curve labeled Narasimha used the expression for Γ given by Eq. (4) whereas the ONERA/CERT labeled model is based on a transition function ϵ_t, which replaces Γ in Eq. (30). This transition function ϵ_t is empirically derived and is discussed in Ref. 5. Figure 1 is a plot of recovery factor vs Reynolds number based on the distance along the surface. Figure 1 demonstrates that the present model does a much better job of predicting the length of the transition zone as well as the peak in the recovery factor. The laminar region is also predicted well. It is believed that the boundary-layer codes were started with a laminar profile just before the transition region and, therefore, the laminar region was never calculated. The recovery factor was assumed to be $\sqrt{Pr}$ and thus resulted in a straight line for the linear combination models. Both the linear combination models and the present constant Pr_t model do a poor job of reproducing the decreasing trend of the recovery factor in the fully turbulent region.

Figure 2 compares the present results of the constant turbulent Prandtl number model to the two-equation transition model of Wilcox as presented in Chang et al.[17] The Wilcox model modifies the production and dissipation terms in the $\tilde{k}$–ω turbulence model to simulate transition. The Wilcox model does a better job of reproducing the peak in the recovery factor than the linear combination models. However, the present model with a constant Pr_t does a slightly better job than the Wilcox model in calculating the recovery factor peak and does a much better job reproducing the

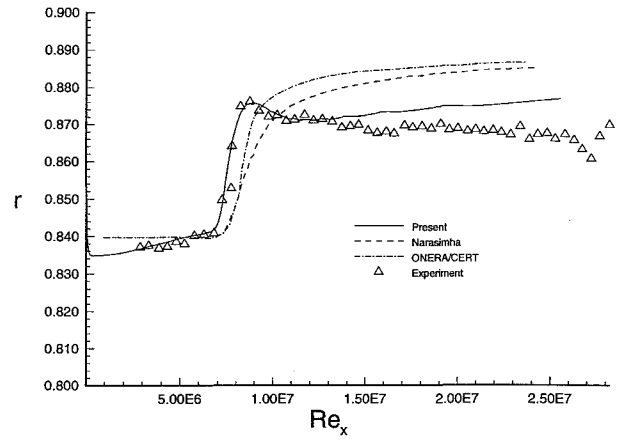

Fig. 1 Flow 3, case 5, constant Pr_t vs previous linear combination models.

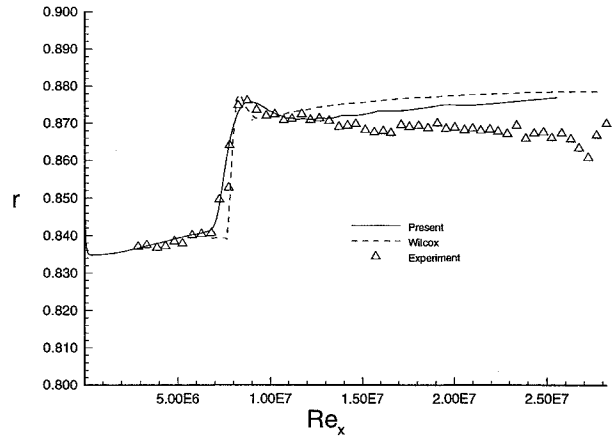

Fig. 2 Flow 3, case 5, constant Pr_t case vs Wilcox model.

transition extent. Additionally, the present method does a slightly better job in the fully turbulent region, although both fail to predict the downward trend in the recovery factor.

The calculation of recovery factor is very sensitive to the choice of the turbulent Prandtl number. Figure 3 is a plot of the current transition model with various choices of the constant Pr_t. By varying the choice of Pr_t by as little as 0.01, very large differences result in the calculation of the recovery factor. This is not too surprising since the recovery factor is such a strong function of the Prandtl number. In Fig. 3, the solid line represents the choice of $Pr_t = 0.89$ which is the choice used for the linear combination models as described in Ref. 5.

Since the recovery factor is sensitive to the value of Pr_t, a closer look was taken at modeling the turbulent diffusivity. As stated previously, using a constant turbulent Prandtl number effectively treats the damping of the thermal boundary layer exactly the same as the damping of the velocity boundary layer. This has no physical basis, especially for high-speed flows where the thermal boundary layer becomes important due to the large temperature gradients in the viscous layer. Following the work of Cebeci,[6] the concept of a variable turbulent Prandtl number was used to define the current eddy-diffusivity model [Eq. (13)]. A typical profile of the variable turbulent Prandtl number is compared in Fig. 4 to the flat-plate measurements of Meier and Rotta.[7] The results of incorporating a variable Pr_t into the present model are compared with the flow 3, case 5 experiment in Fig. 5. As can be seen from the figure, the experimental data in the turbulent region is almost exactly reproduced. Even though the peak in the recovery factor is slightly overpredicted, the transition extent is well predicted.

To determine if the constants used in the specification of the temperature length scale, Eq. (14), are general, the other experiments in the Mach 3.5 cases were computed. Figure 6 gives the results of the present model for the second case, flow 3, case 6. It is clear that the present model accurately reproduces the transition extent, the peak

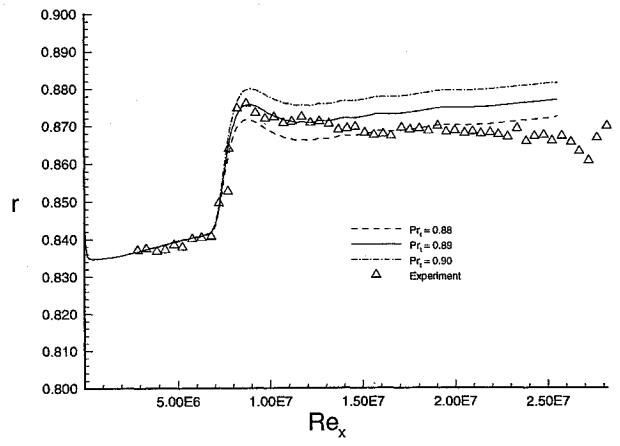

Fig. 3 Flow 3, case 5, turbulent Prandtl number sensitivity.

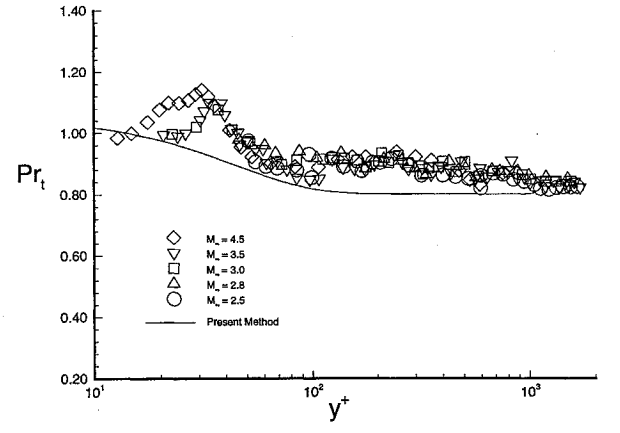

Fig. 4 Flow 3, case 5, one-equation eddy-diffusivity model comparison.

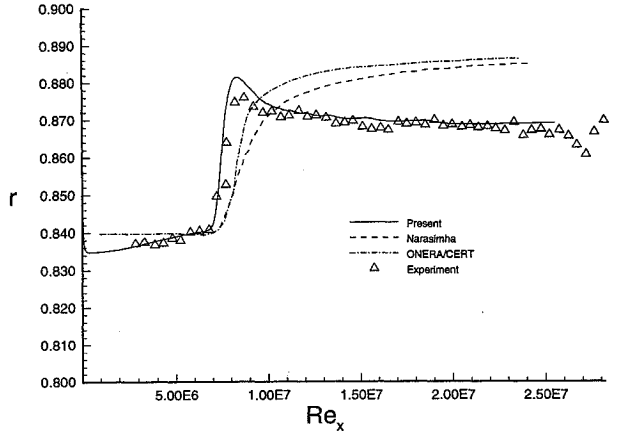

Fig. 5 Flow 3, case 6, one-equation eddy-diffusivity model comparison.

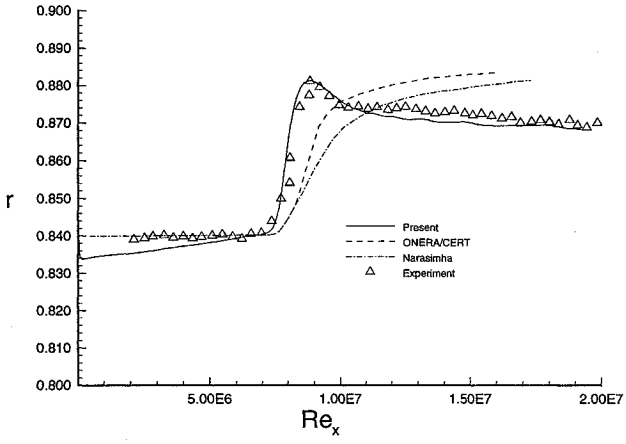

Fig. 6 Flow 3, case 7, one-equation eddy-diffusivity model comparison.

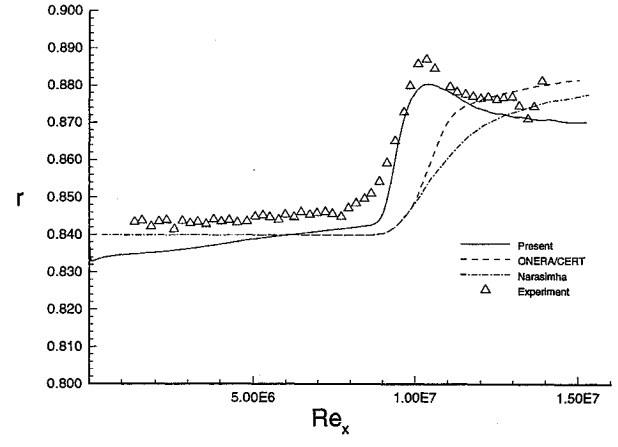

Fig. 7 Flow 3, comparison of measured recovery factor, laminar.

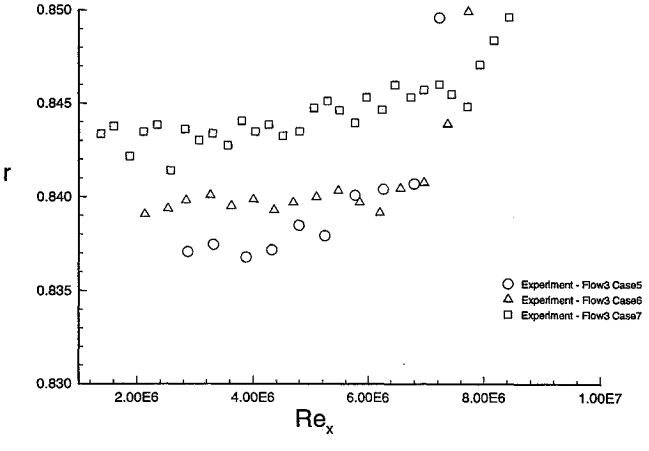

Fig. 8 Experimental Pr_t measurements of Meier and Rotta.

in the recovery factor, and the turbulent region. The results show the extreme differences in the predictions of the present method and the linear combination models. A curious observation in the laminar region can be seen by examining Fig. 6. The experimental data is almost flat in the laminar region whereas the present method predicts a slight increase in the recovery factor. The experimental results shown here were obtained with the same test model as were the results in Fig. 5. However, different values were measured for the recovery factor for the same Reynolds number based on x. This seems to suggest either slight error in the measurements or the model has not reached equilibrium conditions. A similar situation is indicated in Fig. 7, which shows the prediction for the flow 3, case 7 experiment. Even though the transition extent is predicted well, poorer results are obtained in comparison with the previous cases. There is a possible explanation for this. Each of the experiments were carried out with the same test model. A reasonable assumption is that the recovery factor measured should be the same for each of the test cases for the same Re_x, given that laminar flow exists there. Figure 8 demonstrates that each of the cases measured different values for the laminar recovery factor at the same Re_x. As seen from the figure, the flow 3, case 5 experiment measured around 0.837 for the recovery factor, whereas each of the succeeding cases measured values of about 0.840 and 0.844, respectively. This is clearly a discrepancy in the data. If the tests were not allowed to completely reach steady state (adiabatic wall conditions), the measured value of the recovery factor would have been higher than the steady-state value, since the computations assumed adiabatic conditions and consistent values for the recovery factor were computed in the laminar region. As a result, it is suggested that the present method accurately predicts the steady-state value of the recovery factor for the laminar, transitional, and turbulent regions.

In summary, the transitional results presented by Chen et al.[3] are well predicted by the present model. Moreover, the results of the current model illustrate the inadequacies of using a constant turbulent Prandtl number for cases that present recovery factor data. Evidently, the current transition model is the only model presently known that correctly reproduces the trends in the turbulent region for these experiments.[5,17]

Mach 8 Cases

The Mach 8 cases were used to determine the effectiveness of the present model in predicting transitional flows which are characterized by second-mode dominated transition processes. The experiments were carried out by Stetson and Kimmel at AEDC tunnel B and were reported in Ref. 16.

The first case considered is the flared cone case. The surface is flared to produce a constant adverse pressure gradient. The results of the present method are presented in Fig. 9 as the dimensional surface heat flux vs distance along the surface. The experimental data is, in general, reproduced well. The experimental data seems to imply that the heat flux in the turbulent region is either flat or is decreasing, contradicting the trend predicted by theory. This seems to be reinforced by the calculations in Ref. 17. However, Kimmel[16] points out the following:

> An adverse pressure gradient in incompressible flow causes boundary layer thickness to increase and heat transfer to decrease compared to zero-pressure gradient values, but the opposite trends occur in compressible flow. This is primarily because of changes in streamtube size and Mach number in pressure gradients in compressible flow. Consequently, wall shear and heat transfer decrease more slowly with x in an adverse pressure gradient than in zero pressure gradient. A strong enough adverse gradient causes heat transfer and wall shear to increase in the x-direction.

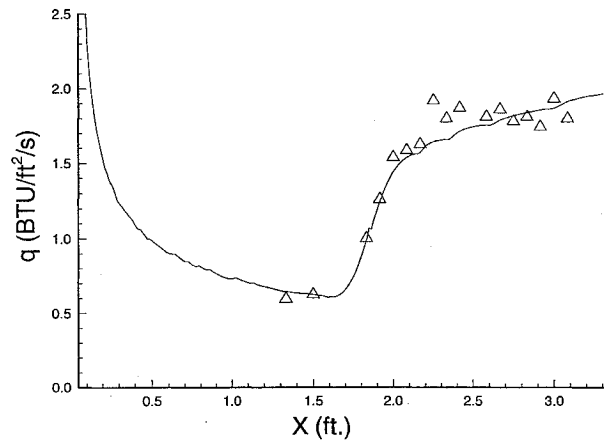

Fig. 9 Mach 8, flared cone, present method.

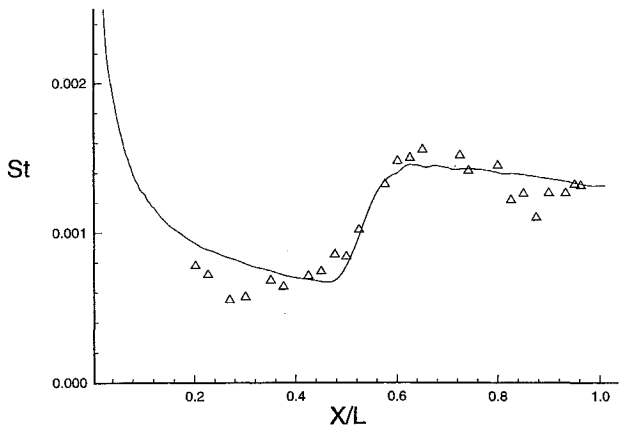

Fig. 10 Mach 8, non flared cone, present method.

Additionally, Kimmel[16] states that the error in the measurements could have been as high as ±10%. It is, therefore, possible that the increase in the heat transfer shown by the present method in the turbulent region is accurate.

The second case of the Mach 8 experiments was the nonflared 7-deg half-angle cone. Figure 10 presents the results of the current transition model. The results are presented as nondimensional heat flux vs nondimensional distance along the surface. The transitional and turbulent regions are reproduced quite well. The discrepancy in the laminar region is most likely experimental error since there is large scatter and no clear transition point. It is also possible that the laminar discrepancy is a result of the high levels of freestream turbulence.

As the comparisons with the Mach 8 cases demonstrate, the second-mode model performs well.

Mach 9 Cases

The next set of data to be considered is that taken in the Imperial College No. 2 Gun Tunnel at Mach 9 by Coleman et al.[20] The data corresponds to natural transition on a flat plate. The tunnel is not considered a quiet tunnel and, as a result, it is not clear how the tunnel noise affects transition and its extent.

All comparisons are made with the data given in Fig. 3 of Ref. 20. Figure 11 compares the prediction of the theory with the cold wall correction indicated in Eq. (9) whereas Fig. 12 corresponds to the present theory without the wall correction. It is seen from the figures that the theory overpredicts the data when the cold wall correction is included and agrees quite well with the measurements when the cold wall correction is removed. Judging by the fact that the theory was in good agreement with the Mach 8 data, it is difficult to explain the cause of the discrepancy in the absence of quantitative characterization of the noise in the tunnel.

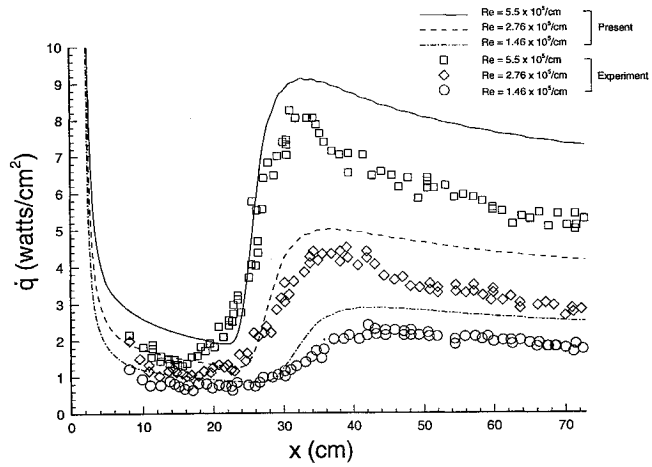

Fig. 11 Mach 9, flat plate, with cold wall correction.

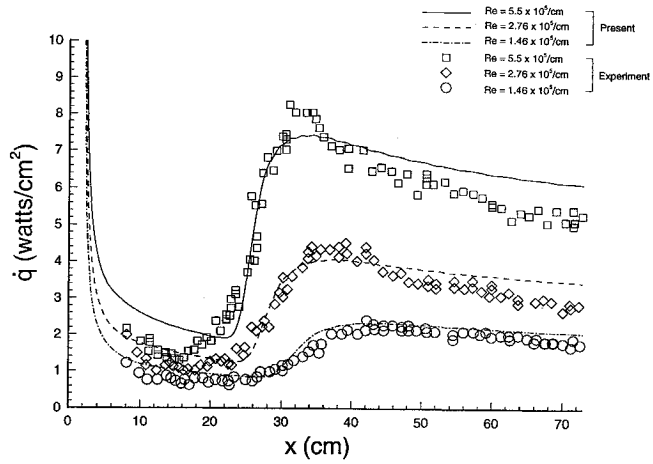

Fig. 12 Mach 8, flat plate, without cold wall correction.

Conclusions

The present transition model is based on the fact that the stress in the transitional region can be expressed as a function of the turbulent and nonturbulent stresses. The nonturbulent stress is due to the presence of laminar fluctuations which are a result of first- and second-mode oscillations. This work has successfully formulated a method in which these laminar disturbances can be accounted for in the computation of a high-speed transitional flow.

The present work successfully demonstrates that effects of second-mode disturbances can be included into the transition model using a form similar to the first-mode disturbance model. The model has been shown to predict first-mode dominated transitional flows accurately and performed better than previous modeling attempts. Additionally, the model has been shown to accurately predict hypersonic transitional flows which are characterized by second-mode dominated transition.

Acknowledgments

This work is supported by NASA's Cooperative Agreement NCCI-22. The authors would like to acknowledge helpful discussions with Ndaona Chokani of North Carolina State University, and Roger Kimmel of Wright Patterson Air Force Base.

References

[1]Young, T. W., Warren, E. S., Harris, J. E., and Hassan, H. A., "New Approach for the Calculation of Transitional Flows," *AIAA Journal*, Vol. 31, No. 4, 1993, pp. 629–636.

[2]Dhawan, S., and Narasimha, R., "Some Properties of Boundary Layer Flow During Transition from Laminar to Turbulent Motion," *Journal of Fluid Mechanics*, Vol. 3, No. 4, 1958, pp. 418–436.

[3]Chen, F.-J., Malik, M. R., and Beckwith, I. E., "Boundary-Layer Transition on a Cone and Flat Plate at Mach 3.5," *AIAA Journal*, Vol. 27, No. 6, 1989, pp. 687–693.

[4]Mitcheltree, R. A., Salas, M. D., and Hassan, H. A. "One-Equation Turbulence Model for Transonic Airfoil Flows," *AIAA Journal*, Vol. 28, No. 9, 1990, pp. 1625–1632.

[5]Singer, B. A., Dinavahi, S. P. G., and Iyer, V., "Testing of Transition-Region Models: Test Cases and Data," NASA CR 4371, May 1991.

[6]Cebeci, T., "A Model for Eddy Conductivity and Turbulent Prandtl Number," *Journal of Heat Transfer*, Vol. 95, Series C, No. 2, May 1973, pp. 227–233.

[7]Meier, H. U., and Rotta, J. C., "Temperature Distributions in Supersonic Turbulent Boundary Layers," *AIAA Journal*, Vol. 9, No. 11, 1971, pp. 2149–2156.

[8]Obremski, H. J., Morkovin, M. V., and Landahl, M., "Portfolio of Stability Characteristics of Incompressible Boundary Layers," AGARDograph 134, March 1969.

[9]Walker, G. J., "Transitional Flow on Axial Turbomachine Blading," *AIAA Journal*, Vol. 27, No. 5, 1989, pp. 595–602.

[10]Anderson, J. D., Jr., *Hypersonic and High Temperature Gas Dynamics*, McGraw-Hill, New York, 1989, pp. 286–295.

[11]Eckert, E. R. G., "Engineering Relations for Heat Transfer and Friction in High-Velocity Laminar and Turbulent Boundary-Layer Flow Over Surfaces with Constant Pressure and Temperature," *Transactions of the American Society of Mechanical Engineers*, Vol. 78, No. 6, 1956, p. 1273.

[12]Mack, L. M., "Boundary Layer Linear Stability Theory," AGARD Rept. 709, June 1986.

[13]Mack, L. M., "Linear Stability Theory and the Problem of Supersonic Boundary-Layer Transition," *AIAA Journal*, Vol. 13, No. 3, 1975, pp. 278–289.

[14]Mack, L. M., "Stability of Axisymmetric Boundary Layers on Sharp Cones at Hypersonic Mach Numbers," AIAA Paper 87-1413, June 1987.

[15]Stetson, K. F., and Kimmel, R. L., "On Hypersonic Boundary-Layer Stability," AIAA Paper 92-0737, Jan. 1992.

[16]Kimmel, R. L., "Experimental Transition Zone Lengths in Pressure Gradient in Hypersonic Flow," *Symposium on Transitional and Turbulent Compressible Flows*, edited by L. D. Kral and T. Zang, Vol. FED 151, American Society of Mechanical Engineers Fluids Engineering Conf., New York, 1993, pp. 117–127.

[17]Chang, C.-L., Singer, B. A., Dinavahi, S. P. G., El-Hady, N. M., Harris, J. E., Streett, C. L., and Wilcox, D. C., "Transition Region Modeling for Compressible Flow," National Aerospace Plane CR 1142, Feb. 1993.

[18]Gaffney, R. L., Jr., Salas, M. D., and Hassan, H. A., "An Abbreviated Reynolds Stress Turbulence Model for Airfoil Flows," AIAA Paper 90-1468, June 1990.

[19]Dey, J., and Narasimha, R., "An Integral Method for the Calculation of 2D Transitional Boundary Layers," Dept. of Aerospace Engineering, Rept. 88 FM 7, Indian Inst. of Science, Bangalore, India, Dec. 1988.

[20]Coleman, G. T., Elfstrom, G. M., and Stollery, S. L., "Turbulent Boundary Layers at Supersonic and Hypersonic Speeds," AGARD-CP-91, Jan. 1972.